JOURNAL OF GEOPHYSICAL RESEARCH, VOL. 95, NO. C7, PAGES 11,547–11,556, JULY 15, 1990

Recurrence in Truncated Boussinesq Models for Nonlinear Waves in Shallow Water

STEVE ELGAR

Department of Electrical and Computer Engineering, Washington State University, Pullman

M. H. FREILICH

Jet Propulsion Laboratory, Pasadena, California

R. T. GUZA

Center for Coastal Studies, Scripps Institution of Oceanography, La Jolla, California

The rapid spatial recurrence of weakly nonlinear, weakly dispersive, progressive shallow-water waves is examined with numerical simulations using a discretized and truncated (i.e., finite number of allowed frequency modes) form of the Boussinesq equations. Laboratory observations of sandbar formation under recurring, mechanically generated monochromatic waves with small Ursell number have motivated others to suggest that recurrence in naturally occurring random waves contributes to the establishment of periodic longshore sandbars on beaches. The present study primarily examines recurrence in wave fields with Ursell number $O(1)$ and characterizes the sensitivity of recurrence to initial spectral shape and number of allowed frequency modes. It is shown that rapid spatial recurrence is not an inherent property of discretized and truncated Boussinesq systems for evolution distances of 10–50 wavelengths. When a small number of Fourier modes are used to represent an initially monochromatic wave field with significant nonlinearity (the Ursell number is $O(1)$), there is a trend toward recurrence of initial modal amplitudes, consistent with the known periodic solutions for a primary wave and its harmonic. However, for 32 modes or more, numerical simulations indicate only a few cycles of a damped recurrence, followed by disordered evolution of the Fourier amplitudes. For initial conditions similar to ocean field measurements of frequency-sorted swell with Ursell number $O(1)$ and many (>300) modes in the numerical model, the Fourier coefficients of the wave field do not recur rapidly. Thus in these cases the predictions of many rapid recurrence cycles by few-mode models is an artifact of severe truncation. On the other hand, even with many allowed modes, pronounced recurrence is predicted when the Ursell number is small and the initial wave field is monochromatic. In this case, few- and many-mode solutions are similar.

1. INTRODUCTION

Variants of the Boussinesq equations [*Peregrine*, 1967] have been proposed as models for unbroken surface gravity waves in shallow water [*Lau and Barcilon* [1972], *Mei and Ünlüata* [1972], *Peregrine* [1972], *Freilich and Guza* [1984], *Liu et al.* [1985], *Elgar and Guza* [1985, 1986], *Boczar-Karakiewicz et al.* [1987], *Rygg* [1988], and others). *Freilich and Guza* [1984] and *Liu et al.* [1985] have developed models based on discretized and truncated versions of the equations. The models take the form of coupled rate equations for a finite number of modes at fixed, equally spaced frequencies. The equations cast in this form are convenient for modeling the shoaling of naturally occurring random wave fields. When initialized at the seaward edge of the shoaling region with observations, the Boussinesq model with many allowed modes accurately predicts the observed evolution of shoaling, nonbreaking waves with a variety of spectral shapes [*Freilich and Guza*, 1984; *Elgar and Guza*, 1985, 1986].

The long-term evolution of systems analogous to weakly dispersive, weakly nonlinear waves has been of interest since the pioneering work of E. Fermi, J. R. Pasta, and S. Ulam [*Fermi et al.*, 1955] indicated that such systems could exhibit rapid periodic recurrence of initial conditions. *Fermi et al.* [1955] numerically simulated a set of coupled nonlinear oscillators with energy initially concentrated in only a few modes. They observed either a quasi-periodic return to the initial amplitudes of the system or a slow increase in the amplitudes of initially small modes at the expense of the initially large primary (Figure 1). This behavior was in contrast with the expected rapid equipartition of energy among all the modes (i.e., thermalization). The anomalously slow randomization of systems of coupled nonlinear oscillators and their quasi-periodic return to initial modal amplitudes is now called FPU recurrence. Many theoretical investigations of recurrence have studied the nonlinear Schrodinger (NLS) equation, which describes narrow-band surface gravity waves in deep water [*Janssen*, 1981, 1983; *Stiassnie and Kroszynski*, 1982; *Lake et al.*, 1977; *Bryant*, 1988]. Using a discretized version of the Zakharov equation (which describes a field of random deepwater waves), *Caponi et al.* [1982] found FPU recurrence for certain initial spectral shapes and found disordered behavior of the modal amplitudes for other initial values. *Caponi et al.* [1982] also studied the effects of the number of modes (and frequency resolution) on the evolution of the Zakharov system. A common feature of the Fermi et al., NLS, Zakharov, and Boussinesq nonlinear systems is that they allow $O(1)$ energy

Paper number 90JC00574.
0148-0227/90/90JC-00574$05.00

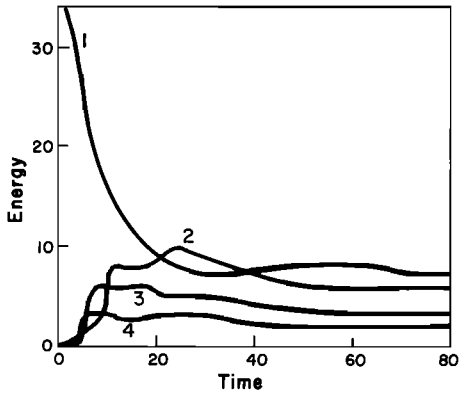

Fig. 1. Energy of the first four Fourier modes of displacement of a nonlinear vibrating string versus evolution time (arbitrary units) from the numerical simulations of *Fermi et al.* [1955, Figure 9].

transfers between modes over large space and time scales. Thus although the systems may periodically return to initial amplitudes, the points of recurrence are separated by periods in which modal amplitudes are significantly different from the initial conditions.

Historically, the nondimensional Ursell number U has been used as a measure of "nonlinearity" in shallow water waves [*Peregrine*, 1967]:

$$U = (a/h)/(kh)^2 \tag{1}$$

where a is a typical amplitude of the sea surface elevation, k is a "typical" wave number, and h is the undisturbed water depth. For $U \ll 1$, nonlinearities are weak, only small energy transfers occur on moderate space or time scales, and $O(1)$ nonlinear effects are possible only over very large scales. For $U \sim 1$, inertial effects (characterized by a/h) are of the same order as dispersive effects ($(kh)^2$), and $O(1)$ energy transfers and phase modifications can occur on moderate space and time scales. The Boussinesq equations are strictly valid for $U = O(1)$, although in practice the equations are quite robust.

There are few detailed laboratory observations of nonlinear recurrence in shallow-water waves with $U = O(1)$, as examined in the present study. Multiple cycles of quasi-periodic returns to initial conditions for initially monochromatic plane waves in intermediate depth have often been observed (e.g., *Madsen* [1971], 3–4 cycles and *Buhr Hansen and Svendsen* [1974], $O(20)$ cycles). In these experiments, $U = O(0.1)$ and the wave dispersiveness was significantly larger than the nonlinearity. The observed modulations in modal amplitudes were not a result of near resonance, and the magnitudes of nonlinear cross-spectral energy transfers were small. For the near-resonant case ($U = O(1)$) of initially monochromatic laboratory waves, *Mei and Ünlüata* [1972] showed that Goda's "appearance distances" (the distance between successive maxima of first-harmonic amplitudes) were in agreement with theory for the recurrence length of a single near-resonant degenerate triad composed of the primary wave and its first harmonic. However, owing to their short laboratory tank, Mei and Ünlüata could observe only a few recurrence cycles. Furthermore, it is unclear whether the observed recurrence was an exact return to initial amplitudes (i.e., FPU recurrence) or if the recurrence cycles were damped, as will be discussed below. Thus there do not appear to be any detailed experiments showing more than three complete recurrence cycles for Ursell numbers greater than 1, even for initial conditions composed of a monochromatic wave. No laboratory experiments address the recurrence of random shallow-water waves.

Several authors [e.g., *Boczar-Karakiewicz and Davidson-Arnott*, 1987; *Davidson-Arnott and Randall*, 1984; and references therein] have suggested that rapid recurrence in the wave field may create spatially periodic longshore-oriented sandbars on very gently sloping beaches. Certainly, sandbars with wavelengths equal to the recurrence length are observed to form in the laboratory when recurring monochromatic waves travel over an erodible bed [*Hulsbergen*, 1974; *Bijker et al.*, 1976; *Boczar-Karakiewicz et al.*, 1987]. Convincing field evidence for recurrence in naturally occuring random long waves is lacking [*Davidson-Arnott and Randall*, 1984), although *Boczar-Karakiewicz et al.*[1987] and *Boczar-Karakiewicz and Davidson-Arnott* [1987] present field data showing possible wave recurrence in association with periodic longshore bars in Lake Huron. In the field situations discussed by *Boczar-Karakiewicz and Davidson-Arnott* [1987], the bottom slope was such that evolution distances of about 20 wavelengths of the primary wave were possible before breaking processes dominated the wave field. Following *Lau and Barcilon* [1972] (see also *Mei and Ünlüata* [1972]), Boczar-Karakiewicz and Davidson-Arnott constructed a coupled wave-sediment model in which the wave field was restricted to a single interacting triad (a primary and its first harmonic). It is well known that such highly truncated Boussinesq wave models predict recurrence on spatial scales of 2–10 wavelengths. In fact, *Boczar-Karakiewicz and Davidson-Arnott* [1987] found that the predicted recurrence length in the wave field corresponded to the observed bar spacing. However, it is not clear whether rapid recurrence behavior is a fundamental characteristic of natural wave fields or whether predictions of rapid recurrence are an artifact resulting from overly truncated models.

In the present study, numerical simulations are used to investigate recurrence in truncated Boussinesq wave models. Specifically, through numerical simulations the sensitivity of recurrence and near-recurrence behavior to the level of truncation and the initial conditions for waves with significant nonlinearity (the Ursell number is $O(1)$) is determined. Evolution distances of tens of wavelengths are examined, characteristic of very gently sloping natural shoaling regions and within the valid length scales of the underlying Boussinesq equations. The numerical results reported below are for constant depth. The nonlinear evolution of shallow-water waves governed by the discretized Boussinesq equations is not strongly dependent on the bottom slope, and numerical solutions of the nonlinear Boussinesq model for waves traveling over a flat bottom are similar to field observations on a gently sloping beach [*Freilich and Guza*, 1984; *Elgar and Guza*, 1986]. Some initial conditions in this study were derived from actual field measurements. Throughout, the parameter ranges used in the numerical simulations are both representative of nearshore conditions and consistent with the assumptions inherent in the derivation of the Boussinesq equations (section 2).

A description of the numerical solution technique, including verification of the numerics, is given in section 3. The numerical simulations are described in section 4. The primary result is that the evolution of waves with $U = O(1)$ is

not dominated by FPU recurrence for distances of $O(50)$ wavelengths. The magnitudes and periodicities of "damped recurrence cycles" observed in the numerical simulations is a function of the number of modes used to represent the wave system in severely truncated models (those with less than 32 modes). As the number of modes used to represent the wave field is increased, the damping of the recurrence cycles also increases. With more than 32 modes the wave evolution becomes insensitive to the number of modes, and an initially sharply peaked power spectrum undergoes only one or two cycles of a damped recurrence. Over large distances ($O(100)$ wavelengths), an initially sharply peaked spectrum becomes featureless. Thus severely truncated Boussinesq models do not accurately represent the evolution of naturally occurring shallow water waves with $U = O(1)$. A discussion and conclusions are given in sections 5 and 6, respectively.

2. Boussinesq Equations

The Boussinesq equations for weakly dispersive, weakly nonlinear, unidirectional shallow-water waves are [*Peregrine*, 1967; *Grimshaw*, 1970]

$$g\eta_x + u_{xt} + \tfrac{1}{2}(u_x^2)_x = \tfrac{1}{2}h(u_{tx}h)_{xx} - \tfrac{1}{6}h^2u_{xxxt}$$
$$\eta_t + (hu_x)_x + (\eta u_x)_x = 0 \tag{2}$$

where g is gravitational acceleration, η is the water surface elevation, u is the depth-averaged velocity potential, h is the water depth, and the subscripts x and t indicate differentiation with respect to space and time, respectively. For waves in a constant depth fluid with no reflection or dissipation, η has the Fourier representation

$$\eta = \sum_{n=1}^{N} a_n(x) \cos(\Phi_n(x) - \omega_n t) \tag{3}$$

where the radian frequency ω_n is equal to $n\Delta\omega$, with $\Delta\omega$ the frequency resolution. The small-amplitude (linear) wave number k_n of (2) is given by

$$(\Phi_n)_x = k_n = (\omega_n/(gh)^{1/2})(1 - h\omega_n^2/3g)^{-1}$$

In shallow water, three-wave interactions are resonant, and the slow spatial evolution of the wave field's Fourier amplitudes a_n and phases ϕ_n is given by

$$\dot{a}_n = \sum_{j=1}^{n-1} a_j a_{n-j} R_{(j,n-j)} \sin(\Phi_j + \Phi_{n-j} - \Phi_n) + \sum_{j=n+1}^{N} a_j a_{j-n} R_{(j,n-j)} \sin(\Phi_j - \Phi_{j-n} - \Phi_n) + \sum_{j=1}^{N-n} a_j a_{n+j} R_{(n+j,-j)} \sin(\Phi_{n+j} - \Phi_j - \Phi_n) \tag{4a}$$

$$\dot{\Phi}_n = \sum_{j=1}^{n-1} \left(\frac{a_j a_{n-j}}{a_n}\right) R_{(j,n-j)} \cos(\Phi_j + \Phi_{n-j} - \Phi_n) - \sum_{j=n+1}^{N} \left(\frac{a_j a_{j-n}}{a_n}\right) R_{(j,n-j)} \cos(\Phi_j - \Phi_{j-n} - \Phi_n) - \sum_{j=1}^{N-n} \left(\frac{a_j a_{n+j}}{a_n}\right) R_{(n+j,j)} \cos(\Phi_{n+j} - \Phi_j - \Phi_n) \tag{4b}$$

where N is the number of modes, the overdot indicates differentiation with respect to the propagation direction (in the present case, the offshore coordinate x), and the coupling coefficients R_n are functions of ω and h (given explicitly by *Freilich and Guza* [1984], equations (21)–(24)]). These equations are the many-mode generalization of the evolution equations first presented by *Armstrong et al.* [1962]. Solutions of (4) for a single primary and its harmonic have also been discussed by *Mei and Ünlüata* [1972], *Lau and Barcilon*, [1972], and *Boczar-Karakiewicz and Davidson-Arnott* [1987].

The order of the underlying Boussinesq equations (2) and the two-scaling technique (equation (3)) restrict the region of spatial validity of the solutions (4). With k as a typical wave number and $\varepsilon = a/h \ll 1$ a nonlinear parameter, the linear solutions are valid for distances less than $O(1/(k\varepsilon))$, the scale over which triads of Fourier modes exchange significant energy. Higher-order terms and processes (e.g., resonant quartets) neglected in (4) restrict the range of the present nonlinear solutions to distances less the $O(1/(k\varepsilon^2))$. For typical values of ε used here ($\varepsilon \sim 0.05$), nonlinear energy exchanges are important after evolution distances of a few wavelengths, while higher-order effects may be significant after $O(60)$ wavelengths. Thus the Boussinesq equations are not formally valid for large evolution distances [*Peregrine*, 1967; *Grimshaw*, 1970; *Freilich and Guza*, 1984], and moreover, dissipation and interactions between the waves and the bottom are not included in the model but may be important for long evolution distances in the field [*Miles*, 1983, and references therein]. The present work focuses on evolution distances of 10–50 wavelengths.

Given a set of initial amplitudes and phases, the model (4) can be integrated numerically, yielding Fourier coefficients of sea surface elevation at arbitrary distances from the initial conditions. Initial conditions used here consisted of various power spectral shapes, including idealized narrow-band and broadband spectra as well as spectra based on direct ocean measurements (section 4). The evolution of the sea surface is not strongly dependent on the initial phases if, as occurs at the seaward edge of the shoaling region, the initial system is nearly linear [*Freilich and Guza*, 1984; *Elgar and Guza*, 1986]. In all the cases discussed in section 4 the initial amplitudes were coupled with random Fourier phases.

3. Verification of the Numerical Integration Technique

Equations (4) were integrated at the San Diego Supercomputer Center on a Cray XMP/48 supercomputer with 64-bit word length and approximately 14 decimal places of accuracy. Three standard numerical integration techniques were used: Bulirsch-Stoer, Runge-Kutta-Merson, and Adams-Bashforth-Moulton [cf. *Press et al.*, 1986]. Differences between the results from different integration schemes were

measured (on a mode-by-mode basis) as the magnitude of the difference between the complex Fourier coefficients predicted by each scheme at an evolution distance of 75 wavelengths. The convergence tolerances finally accepted produced no more than 0.8% difference (and for most frequency bands, less than 0.2%) in the Fourier coefficients. Since it was the fastest, the Runge-Kutta-Merson scheme was used for the results presented here. The total linear energy flux varied less than 1% for evolution distances of more than 75 wavelengths.

The evolution equations (4) support nonlinear waves of permanent form. Numerical integrations with initial conditions corresponding to such waves were also used to validate the accuracy of the numerical integration technique. Waves of permanent form have no amplitude evolution and have constant phase speed C_p. Setting $\dot{a}_n = 0$ and $\dot{\Phi}_n = (\omega_n/C_p) - k_n$, the system (4) becomes a set of simultaneous nonlinear algebraic equations with one free parameter. This parameter was selected to be the amplitude of the primary (the lowest-frequency mode in this example) allowing variation in the Ursell number. In this case k in (1) is taken to be the wave number of the primary, and the amplitude a is defined here as one-half the significant wave height of a Gaussian wave field

$$a = 2\left\{\sum_{n=1}^{N} a_n^2/2\right\}^{1/2} \tag{5}$$

The set of algebraic rate equations was solved iteratively using cnoidal wave amplitudes and phases as an initial guess (cnoidal waves are exact solutions to (2), while (3) and (4) are approximate solutions). This solution technique can in principle obtain the Fourier coefficients for any number of modes (see also *Bryant* [1974]), but the present solutions were truncated after 31 modes (the power in mode 31 was at least 5 orders of magnitude less than that in mode 1). The power spectrum and wave profile for a discretized Boussinesq equation wave of permanent form (DBWPF) with $U = 14$ are very similar to those of a cnoidal wave with the same wavelength and wave height (Figure 2). In the limit as $U \to 0$, the DBWPF wave approaches a cnoidal wave. The two wave profiles are virtually indistinguishable for $U = 1$.

With initial conditions corresponding to DBWPF and $U = 14$ the modal amplitudes varied by less than 0.1% over an evolution distance of approximately 100 wavelengths (Figure 3*a*). (Even this slight monotonic variation in amplitude can be removed by increasing the convergence criterion of the numerical integration routines beyond that used for the results presented here.) On the other hand, initial conditions consisting of a true cnoidal wave (Figure 3*b*) or a DBWPF power spectrum coupled with random Fourier phases (Figure 3*c*) do not satisfy the conditions for a wave of permanent form, and the power spectra evolve. For both these cases the power in each of the first three Fourier modes varied by an order of magnitude as the wave field evolved. The stability of the DBWPF suggests that the results reported here are numerically accurate.

4. RESULTS

In this section the long-term evolution of the wave field is examined. The results of numerical simulations illustrating the sensitivity of damped recurrence behavior on the number of modes and on the spectral shape of the initial conditions are presented in sections 4.1 and 4.2, respectively. Results for an initial spectrum derived from ocean field measurements follow in section 4.3. In all cases the initial conditions satisfied the restrictions required for the Boussinesq equations to be formally valid (i.e., $U = O(1)$).

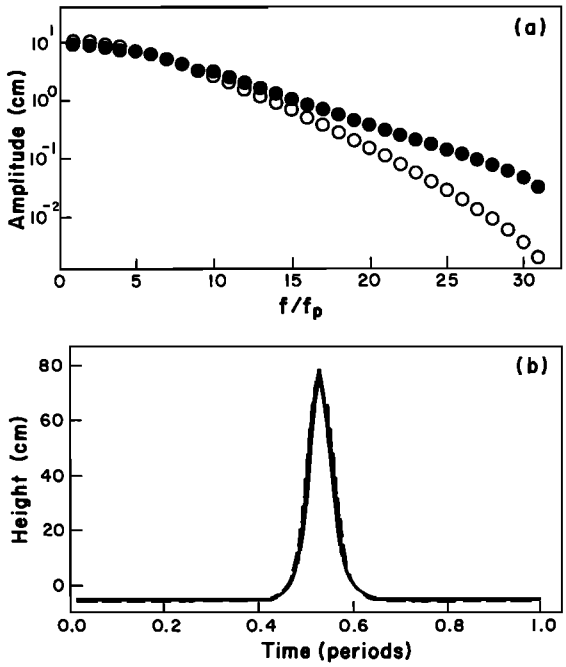

Fig. 2. Comparison of waves of permanent form for $U = 14$. (*a*) Modal amplitudes versus frequency (f_p is the frequency of the primary spectral peak). Solid circles are for the discretized Boussinesq equation; open circles are for the cnoidal wave of the same wavelength and height. (*b*) One period of sea surface elevation. The solid curve is for the discretized Boussinesq equation; the dashed curve is for the cnoidal wave.

4.1. *Effect of the Number of Modes*

A series of simulations was performed in which the wave field was modeled using between 4 and 256 Fourier modes. Each initial spectrum ($x = 0$) consisted of a single large primary peak at $f = 0.0625$ Hz (where $f = \omega/2\pi$) and between 3 and 255 background modes with amplitudes 2 orders of magnitude lower than that of the primary peak. The highest (cutoff) frequency in all cases was $f = 0.25$ Hz, and thus the frequency resolution increased with increasing number of modes. Random initial phases were assigned to each mode, and the depth was chosen arbitrarily to be $h = 2.0$ m. The initial amplitudes (~9 cm) of the primary peak and the background modes corresponded to $U = 1.33$, where the wave number was determined by the linear Boussinesq dispersion relation at the frequency corresponding to the centroid of the power spectrum.

The evolution of the amplitude of the initial primary peak ($f = 0.0625$ Hz) is shown in Figure 4*a* as a function of the number of modes, N. For a single triad (not shown) the evolution equations have strictly periodic solutions [*Armstrong et al.*, 1962]. For $N = 4$ the amplitude evolution is nearly periodic, with the amplitude of the initial peak returning to within 15% of its initial value approximately every 14 wavelengths. However, the trend toward recurrence decreases as the number of modes increases. For 32 modes or

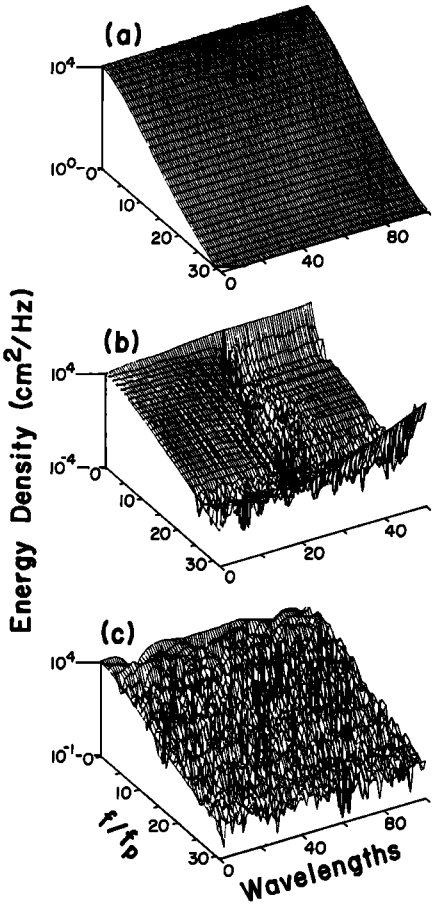

Fig. 3. Power spectra versus evolution distance (units of wavelengths, L, of the initial power spectral primary peak frequency) for $U = 14$. (a) Discretized Boussinesq equation waves of permanent forms, (b) cnoidal wave initial conditions, and (c) waves with the same Fourier amplitudes as waves of permanent form, but with random Fourier phases at the initial condition.

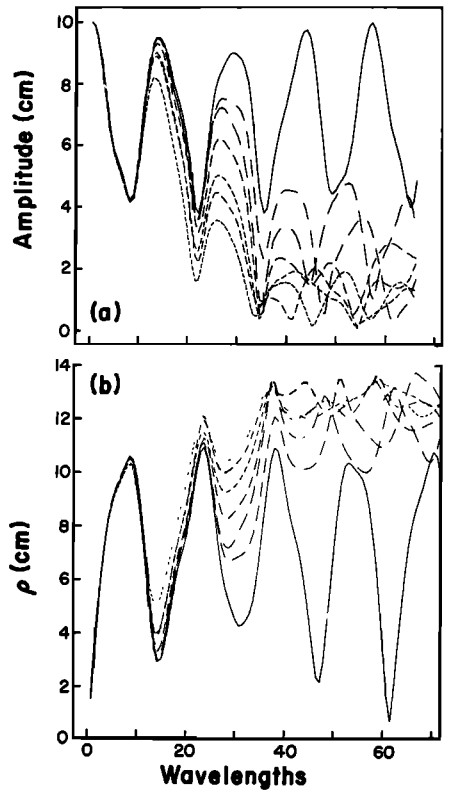

Fig. 4. (a) Amplitude of the initial spectral primary peak frequency and (b) the root-sum-squared difference (equation (6)) versus evolution distance for the initial condition of a single primary peak within a low-level background (section 4.1). The solid curve is for the case of four Fourier modes, and the dashes decrease in size as the number of modes increases from 4 to 256 by factors of 2. The various curve types are best distinguished from each other near $x =$ 30 wavelengths where, from top to bottom, the amplitudes decrease (Figure 4a) and ρ increases (Figure 4b) in the order 4, 16, 8, 32, 128, 64, and 256 modes, respectively.

more, the primary amplitude undergoes two damped recurrence cycles, each about 14 wavelengths long, and then the evolution becomes quite disordered (Figure 4a).

The degree of "recurrence" of the entire spectrum as a function of propagation distance is quantified as the root-sum-squared deviation between the initial and evolved amplitudes, $\rho(x)$, given by

$$\rho(x) = \left\{ \sum_{n=1}^{N} [a_n(x) - a_n(0)]^2 \right\}^{1/2} \qquad (6)$$

where $\rho(s) = 0$ corresponds to perfect amplitude recurrence, and increasing values of $\rho(x)$ indicate increasingly larger deviations from the initial conditions. For wave fields with energy concentrated in a narrow band of frequencies (e.g., Figure 4a), the evolution of $\rho(x)$ (Figure 4b) closely parallels the evolution of the amplitudes near the spectral peak. There is little trend toward recurrence (decrease in $\rho(x)$ values) for propagation distances beyond approximately 30 wavelengths for $N \geq 32$ (Figure 4b).

The evolution of the harmonics of the spectral peak is similar to that of the primary, as is shown in Figure 5 for $N = 256$. Harmonic amplitudes undergo quasi-periodic recurrence for $N = 4$, and as the number of modes increases, the recurrence is damped. For 32 modes or more the evolution of harmonic amplitudes is quite disordered after about 30 wavelengths of the initial primary spectral peak.

Although the simulations indicate that recurrence proper

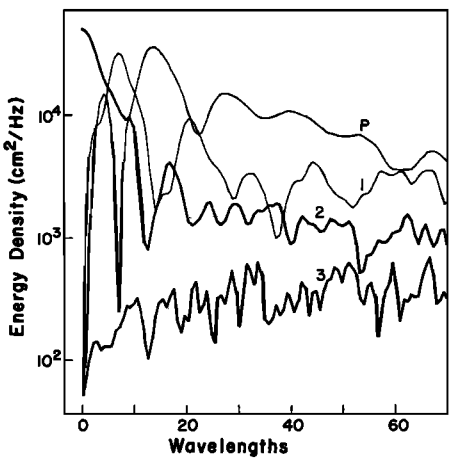

Fig. 5. Power spectral density of the initial primary peak frequency (P) and its first three harmonics (1–3) versus evolution distance for the initial condition of a single primary peak within a low-level background (256 modes, section 4.1).

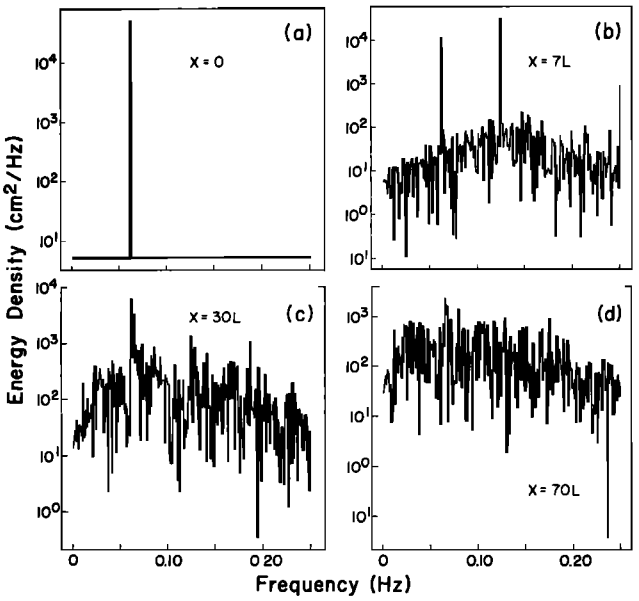

Fig. 6. Power spectra for the initial condition of a single primary peak within a low-level background (256 modes, section 4.1) for (*a*) $x = 0$, (*b*) $x = 7L$, (*c*) $x = 30L$, and (*d*) $x = 70L$.

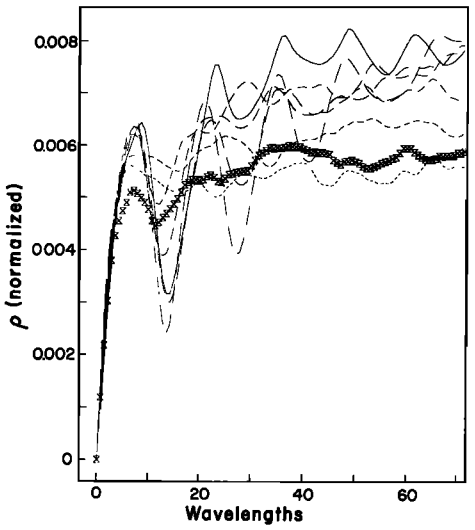

Fig. 7. Root-sum-squared (rss) difference (normalized by the rss difference between the initial spectrum and a fully white spectrum with the same total variance) versus evolution distance for the initial conditions of section 4.2 The solid curve is for $N_p = 1$, and the dashes decrease in length as N_P increases from 1 to 64 by factors of 2. The thick cross-hatched curve is for the ocean field data initial spectrum, case 3 in Table 1 (section 4.3).

ties of the initially very narrow spectra studied here are somewhat sensitive to the number of modes (N) for small N, there is no strong dependence on N for $N \geq 32$.

The spatial evolution of sea surface elevation spectra for the 256-mode case is illustrated in Figure 6. After initial cross-spectral energy exchanges confined primarily to the harmonics of the initial primary peak, energy spreads to all modes, and the spectrum flattens substantially, becoming relatively featureless.

4.2. *Effect of Spectral Bandwidth*

The effect of spectral bandwidth on recurrence is illustrated by simulations with initial conditions consisting of flat spectra with various bandwidths. The spectral amplitudes for this set of simulations were

$$a_n = (1/N_p)^{1/2} a \qquad 64 - \frac{N_p}{2} + 1 < n < 64 + \frac{N_p}{2}$$

$$a_n = a_b \qquad \text{otherwise}$$

where N_p is the number of modes within the initial spectral peak, centered at $f = 0.0625$ Hz ($n = 64$) as in section 4.1. For each simulation $a_b = 0.01a$, where a_b is the background spectral amplitude $h = 2$ m, and $U \simeq 2$ (based on the wave number corresponding to the power spectral centroidal frequency), thus fixing the value of a. In each of these comparisons, N is equal to 256, and the frequency resolution was $\Delta f = 10^{-3}$ Hz. Ten realizations of random initial phases were simulated for each choice of peak bandwidth, with the resulting spectra averaged.

The case of $N_p = 1$ here corresponds to the monochromatic initial condition with $N = 256$ discussed in section 4.1. Equations (4) having initial spectra with $1 \leq N_p \leq 64$ were integrated, and in each case the solution eventually evolved to a nearly featureless, flat spectrum. However, as is shown in Figure 7, the persistence of initial damped recurrence cycles is a function of the initial bandwidth. Initially narrow-banded spectra undergo more recurrence cycles, and the damping is reduced (i.e., $\rho(x)$) values return more closely to 0) relative to the evolution of initially broader-banded spectra. The locations of the first few extrema in the individual $\rho(x)$ curves occur at approximately the same evolution distance, essentially independent of initial bandwidth.

Several cases of white ($a_n = \text{const}$, $1 \leq n \leq 256$) initial spectra were simulated, with $2 \leq U \leq 20$. In each instance there was no major change in spectral shape over evolution distances similar to those discussed above. Power spectral peaks varied during evolution by as much as a factor of 4 from their initial levels, but with no obvious pattern. At no evolution stage did the power spectrum closely resemble the initial spectral shape.

4.3. *Narrow-Band Ocean Data*

Ocean measurements in 4-m water depth provided the mean initial spectral shape ($x = 0$ in Figure 8) for another set of numerical simulations. This narrow-band power spectrum (primary spectral peak at $f = 0.06$ Hz) is typical of frequency-sorted swell from a distant storm. Five cases with this initial spectral shape were investigated (Table 1). The first three cases correspond to different depths ($h = 1.0$, 1.5, and 2.0 m). Although the initial relative amplitudes of Fourier

TABLE 1. Parameters for the Five Initial Conditions of Section 4.3.

Case	U	a/h	kh	h, m
1	1.33	0.033	0.16	1.0
2	1.33	0.050	0.19	1.5
3	1.33	0.067	0.22	2.0
4	1.78	0.067	0.19	1.5
5	2.68	0.067	0.16	1.0

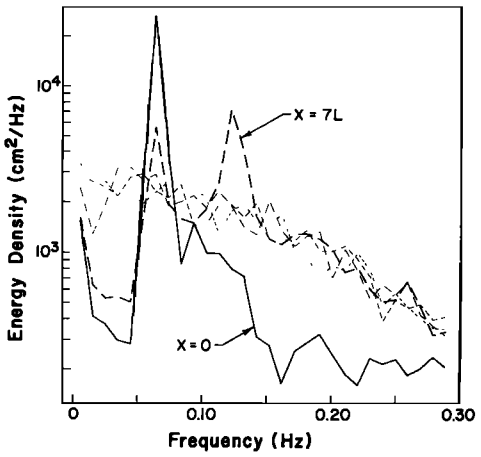

Fig. 8. Power spectral shape used for the five initial conditions (x = 0) of Table 1 (solid curve) and for the case 3 simulations at evolution distances of 7L (longest dashes), 30L (second longest dashes), 50L (second shortest dashes), and 70L (shortest dashes), where L = 70 m, the wavelength of the spectral primary peak frequency at x = 0 for case 3 (U = 1.33, kh = 0.22 (Table 1)). For purposes of display, spectral levels from ten neighboring frequency bands were merged.

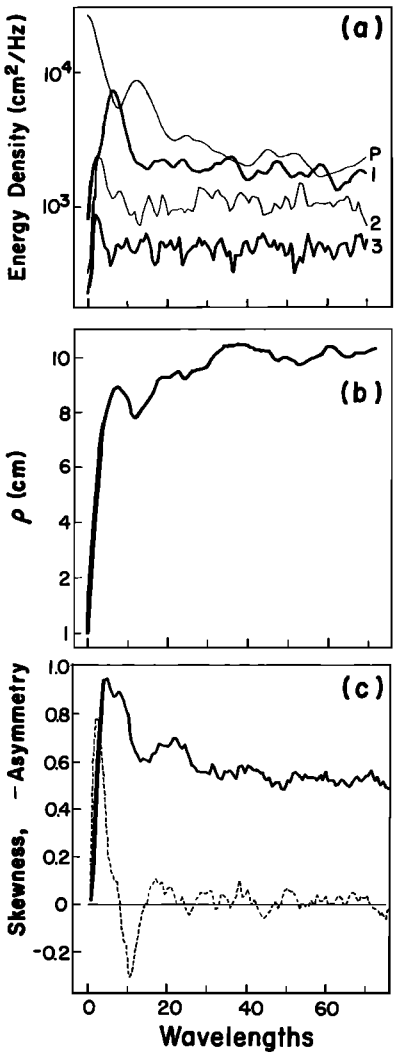

Fig. 9. (*a*) Power spectral density of the initial primary peak frequency (P) and its first three harmonics (1–3), (*b*) root-sum-squared difference, and (*c*) skewness (solid curve) and asymmetry (dashed curve) versus evolution distance for case 3 (U = 1.33, kh = 0.22 (Table 1)).

modes were the same for each case, a scaling factor was applied to all amplitudes so that each case had an initial Ursell number of 1.33. Two additional cases of a/h = 0.067 were investigated, with U = 1.78 and U = 2.68. In each case, five separate, consecutive 17-min time series of measured sea surface elevation were used to generate the initial spectral shapes, and the results of the numerical integrations were ensemble averaged. There were 307 Fourier modes in these cases, with frequency resolution $\Delta f = 10^{-3}$ Hz and a high-frequency cutoff of f = 0.3 Hz. Increasing the high-frequency cutoff to f = 0.48 Hz (491 modes) did not alter the results presented here.

Evolution of the spectra (Figure 8), the power of the initial primary spectral peak (f = 0.06 Hz) and its first three harmonics, the root-sum-squared difference $\rho(x)$, and third moments of the sea surface (possibly related to the direction of net sediment transport (*Bailard* [1981] and many others) (Figure 9) are shown for case 3 (Table 1). These results for the ocean-derived initial conditions are very similar to those for the idealized case of an initially very narrow spectrum with many background modes (section 4.1 and Figures 5 and 6). The power in the primary decreases during the first eight wavelengths ($0 \le x \le 8L$), then increases to a level one-third that of the initial value (at x = 12 L) and subsequently decreases again (Figure 9). There is a slight increase at x = 24L, but for greater propagation distances the power in the primary spectral peak does not vary by more than a factor of 2 from a value of about one-tenth the initial (x = 0) value. All three harmonic amplitudes initially increase concomitantly with the decrease in the primary (Figure 9), and all three subsequently decrease as the primary increases near x = 8–12L. Although the power in each of the three harmonics continues to vary with distance, there is no obvious pattern to the variations and certainly no evidence of recurrence of the initial values. At x = 0 the power of the primary is more than 100 times greater than the power of the third harmonic. However, after 30 wavelengths the difference is less than a factor of 10 and remains relatively constant for the duration of the simulation.

During the initial stages of evolution the harmonics of the primary grow (e.g., x = 7L in Figure 8). As the wave field evolves further, spectral valleys are filled in at the expense of spectral peaks. After 30 wavelengths the power spectra are essentially featureless, and almost all traces of the sharp primary spectral peak and its harmonics are gone. The normalized $\rho(x)$ values for this case (shown in Figure 7) are similar to those for an idealized flat spectrum with bandwidth between 0.03 and 0.06 Hz (the N_p = 32 and N_p = 64 mode cases of section 4.2 and Figure 7), although the initial spectra differ in detail.

The pattern of spatial evolution of the amplitudes of the initial power spectral primary peak (Figure 10*a*) and $\rho(x)$ (Figure 10*b*) is similar to that shown in Figures 7–9 for all five cases. There is no evidence of recurrence of the initial conditions over the evolution distances considered here.

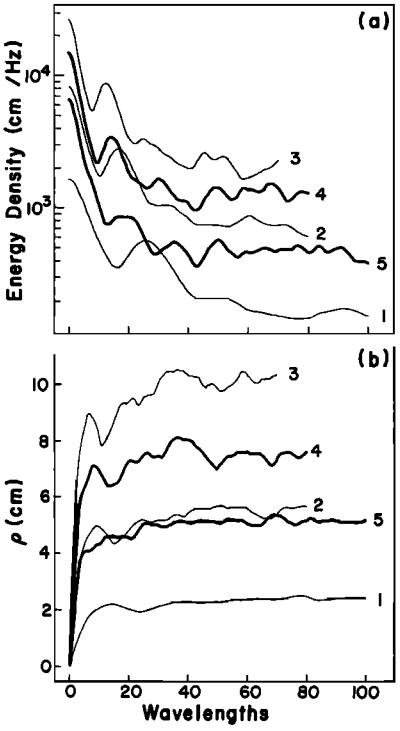

Fig. 10. (*a*) Power spectral density of the initial spectral primary peak frequency and (*b*) root-sum-squared difference versus evolution distance for cases 1–5 (Table 1).

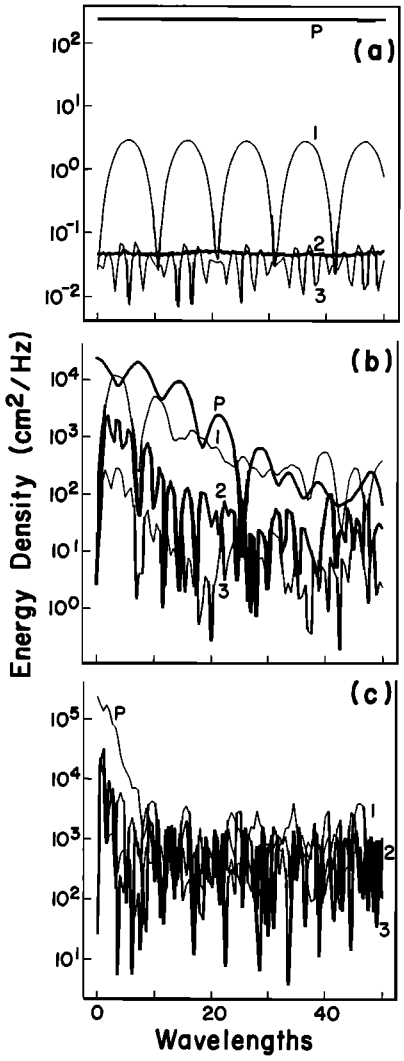

Fig. 11. Power spectral density of the initial primary peak frequency P and its first three harmonics (1–3) versus evolution distance for the initial condition of a single primary peak within a low-level background (256 modes, section 4.1). (*a*) $U = 0.1$, (*b*) $U = 1.0$, and (*c*) $U = 3.1$. For all cases, $kh = 0.34$.

5. Discussion

Previously reported laboratory studies (section 1) showing more than three nearly periodic cycles in harmonic amplitudes were all for small Ursell number. These multiple cycles are predicted by the Boussinesq model with small U, many allowed modes, and an initially monochromatic plane wave. For example, with $U = 0.10$ and 256 allowed modes, five nearly identical cycles are predicted in an evolution distance of 50 wavelengths, in contrast to the damped cycles predicted for an initial plane wave with $U = 1.0$ and the absence of recurrence cycles for $U = 3.1$, as shown in Figure 11. The distinction between $U = O(0.1)$ and $U = O(1)$ is critical. For small Ursell number the harmonics never reach amplitudes comparable to the initial primary (compare Figure 11*a* with Figures 11*b* and 11*c*) because the relatively weak nonlinearities cannot produce significant energy exchanges during the recurrence length scale.

For waves in deep water the modulation length scale of harmonic amplitudes is comparable to the wavelength of the primary. Thus "recurrence" cycles occur relatively rapidly, and many cycles can be observed in short laboratory basins ($O(20)$ primary wavelengths long), although the harmonics are always small in amplitude relative to the primary wave. When $U = O(1)$ and $(kh)^2 \ll 1$, the recurrence length of an isolated triad becomes longer relative to a primary wavelength [*Mei and Ünlüata*, 1972], and thus longer basins are required to observe many recurrence cycles. The numerical results presented here indicate that when $U = O(1)$ the recurrence cycles of even an initially monochromatic plane wave are damped (Figure 11). It would be of interest to test these predictions in a very long (30 wavelengths) laboratory flume using waves not strongly influenced by viscosity.

Figure 12 illustrates the effect of decreasing U on the evolution of the broader-banded, naturally occurring initial spectral shape shown in Figure 8. In contrast to the case of an initially monochromatic wave train, decreasing U for this finite-bandwidth initial spectrum does not significantly alter the overall levels of spatial recurrence, as can be seen by comparing $\rho(x)$ for $U = 1.33$ (Figure 9) with $\rho(x)$ for $U = 0.14$ (Figure 12). However, for this initial spectral shape, smaller U does result in smaller maximum amplitudes of harmonics and third moments (Figure 12) relative to larger U (Figure 9).

The implications of these results with respect to bar formation on natural beaches are not clear. Further modeling is necessary to determine whether the highly damped cycles predicted by the many-mode model are strong enough to form bars in the underlying sediment. It is apparent that observations (and truncated models) of bar formation in the laboratory with recurring monochromatic plane waves and relatively small U cannot be extrapolated to random waves, particularly if $U = O(1)$.

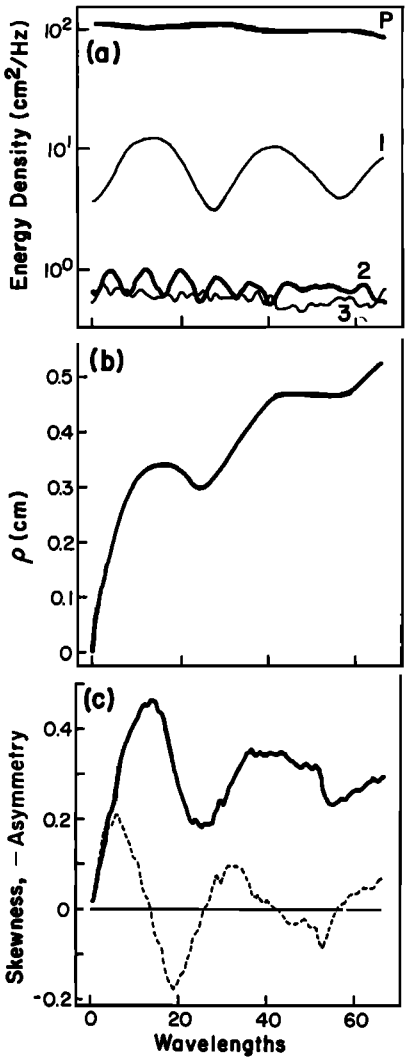

Fig. 12. (*a*) Power spectral density of the initial primary peak frequency (P) and its first three harmonics (1–3), (*b*) root-sum-squared difference, and (*c*) skewness (solid curve) and asymmetry (dashed curve) versus evolution distance for the initial condition with the same spectral shape as shown in Figure 8 (field data), but with $U = 0.12$, $kh = 0.22$.

6. Conclusions

The primary result of this study is that highly truncated Boussinesq models of resonant ($U = O(1)$) shallow-water ocean surface gravity waves predict rapid, multiple recurrence cycles, but that this is an artifact dependent on the number of allowed modes. For initial conditions consisting of essentially all energy concentrated in a single mode, damping of the recurrence cycles increases as the number of low-power background modes increases. When more than 32 modes are allowed in the model, the recurrence behavior is relatively insensitive to the number of allowed modes. The predicted evolution of the wave model with many allowed modes is similar to that found in some of the numerical examples of *Fermi et al.* [1955] (compare Figure 1 with Figure 5) for systems of nonlinear strings.

Damping is even more rapid when the initial energy-containing portion of the spectrum has realistic (with respect to ocean data) bandwidth. Very narrow band spectra undergo more recurrencelike cycles before the spectra flatten than do broad spectra (Figure 7). Initially broad-banded spectra remain so. For the case of an initially narrow spectrum derived from ocean field measurements and $U = O(1)$, there is some tendency for one damped recurrence cycle before the spectrum becomes broad banded, with spectral valleys filled in at the expense of spectral peaks (Figures 8–10). Third moments of the sea surface also do not recur strongly for the $U = O(1)$ initial conditions studied here (Figure 9), although there is somewhat less damping in third moments when $U = O(0.1)$ (Figure 12).

Models allowing many modes can accommodate finite bandwidth and do not exhibit significant sensitivity to the exact number of modes used. On the basis of the numerical simulations it appears that natural fields with $U = O(1)$ would not exhibit rapid, multiple recurrence cycles.

Acknowledgments. This research was supported by the Physical Oceanography Program of the National Science Foundation. Portions of the research were performed at the Jet Propulsion Laboratory, California Institute of Technology, under contract to NASA. The computations were performed at the San Diego Supercomputer Center (supported by NSF). The center's staff provided extensive and invaluable help with numerous aspects of the computations. Gloria Sebert and Erika Johnston (supported by the NSF REU program) made substantial contributions to the data reduction effort.

References

Armstrong, J. A., N. Bloembergen, J. Ducuing, and P. S. Persham, Interactions between light waves in a nonlinear dielectric, *Phys. Rev.*, *127*, 1918–1939, 1962.

Bailard, J. A., An energetics total load sediment transport model for a plane sloping beach, *J. Geophys. Res.*, *86*, 10,938–10,954, 1981.

Bijker, E. W., E. van Hijum, and P. Vellinga, Sand transport by waves, in *Proceedings of the 15th International Conference on Coastal Engineering*, pp. 1149–1166, American Society of Civil Engineers, New York, 1976.

Boczar-Karakiewicz, B., and R. Davidson-Arnott, Nearshore bar formation by nonlinear wave processes—A comparison of model results and field data, *Mar. Geol. 77*, 287–304, 1987.

Boczar-Karakiewicz, B., J. L. Bona, and D. L. Cohen, Interaction of shallow-water waves and bottom topography, in *Dynamical Problems in Continuum Physics*, vol. 4, *Mathematics and its Application*, edited by J. L. Bona, pp. 131–176, Springer-Verlag, New York, 1987.

Bryant, P. J., Stability of periodic waves in shallow water, *J. Fluid Mech.*, *66*, 81–96, 1974.

Bryant, P. J., Cyclic recurrence in nonlinear unidirectional ocean waves, *J. Fluid Mech.*, *192*, 329–337, 1988.

Buhr Hansen, J., and I. A. Svendsen, Laboratory generation of waves of constant form, in *Proceedings of the 14th International Conference on Coastal Engineering*, pp. 321–329, American Society of Civil Engineers, New York, 1974.

Caponi, E. A., P. G. Saffman, and H. C. Yuen, Instability and confined chaos in a nonlinear dispersive wave system, *Phys. Fluids*, *25*, 2159–2166, 1982.

Davidson-Arnott, R., and D. C. Randall, Spatial and temporal variations in spectra of storm waves across a barred nearshore, *Mar. Geol.*, *60*, 15–30, 1984.

Elgar, S., and R. T. Guza, Shoaling gravity waves: Comparisons between field observations, linear theory and a nonlinear model, *J. Fluid Mech.*, *158*, 47–70, 1985.

Elgar, S., and R. T. Guza, Nonlinear model predictions of bispectra of shoaling surface gravity waves, *J. Fluid Mech.*, *167*, 1–18, 1986.

Fermi, E., J. R. Pasta, and S. Ulam, Studies of nonlinear problems, *Rep. LA-1940*, Los Alamos Natl. Lab., Los Alamos, N. M., 1955. (Also in *Collected Works of Enrico Fermi*, vol. 2, edited by E. Segre, p. 978, University of Chicago Press, Chicago, Ill., 1962).

Freilich, M. H., and R. T. Guza, Nonlinear effects on shoaling surface gravity waves, *Philos. Trans. R. Soc. London, Ser. A*, *311*, 1–41, 1984.

Grimshaw, R., The solitary wave in water of variable depth, *J. Fluid Mech.*, *42*, 639–656, 1970.

Hulsbergen, C. H., Origin, effect, and suppression of secondary waves, in *Proceedings of the 14th International Conference on Coastal Engineering*, pp. 392–411, American Society of Civil Engineers, New York, 1974.

Janssen, P. A. E. M., Modulational instability and the Fermi-Pasta-Ulam recurrence, *Phys. Fluids*, *24*, 23–26, 1981.

Janssen, P. A. E. M., Long-time behaviour of a random inhomogeneous field of weakly nonlinear surface gravity waves, *J. Fluid Mech.*, *133*, 113–132, 1983.

Lake, B. M., H. C. Yuen, H. Rungaldier, and W. Ferguson, Nonlinear deep-water waves: Theory and experiment, 2, Evolution of a continuous wave train, *J. Fluid Mech.*, *83*, 49–74, 1977.

Lau, J., and A. Barcilon, Harmonic generation of shallow water waves over topography, *J. Phys. Oceanogr.*, *2*, 405–410, 1972.

Liu, P., S. Yoon, and J. Kirby, Nonlinear refraction-diffraction of waves in shallow water, *J. Fluid Mech.*, *153*, 184–201, 1985.

Madsen, O. S., On the generation of long waves, *J. Geophys. Res.*, *76*, 8672–8683, 1971.

Mei, C. C., and U. Ünlüata, Harmonic generation in shallow water waves, in *Waves on Beaches*, edited by R. E. Meyer, pp. 181–202, Academic, San Diego, Calif., 1972.

Miles, J., Wave evolution over a gradual slope with friction, *J. Fluid Mech.*, *133*, 207–216, 1983.

Peregrine, D. H., Long waves on a beach, *J. Fluid Mech.*, *27*, 815–827, 1967.

Peregrine, D. H., Equations for water waves and the approximations behind them, in *Waves on Beaches*, edited by R. E. Meyer, pp. 95–122, Academic, San Diego, Calif., 1972.

Press, W. H., B. P. Flannery, S. A. Teukolsky, and W. T. Vettering, *Numerical Recipes, The Art of Scientific Computing*, 818 pp., Cambridge University Press, New York, 1986.

Rygg, O., Nonlinear refraction-diffraction of surface waves in intermediate and shallow water, *Coastal Eng.*, *12*, 191–211, 1988.

Stiassnie, M., and U. I. Kroszynski, Long-time evolution of an unstable water-wave train, *J. Fluid Mech.*, *116*, 207–225, 1982.

S. Elgar, Department of Electrical and Computer Engineering, Washington State University, Pullman, WA 99164.

M. H. Freilich, Jet Propulsion Laboratory, 300–323, Pasadena, CA 91109.

R. T. Guza, Center for Coastal Studies, Scripps Institution of Oceanography, A-009, La Jolla, CA 92093.

(Received October 10, 1989;
revised March 5, 1990;
accepted March 5, 1990.)